Explosive Coalescence of Magnetic Islands and Particle Acceleration

T. Tajima*, and J.-I. Sakai**

Abstract

An explosive reconnection process associated with the nonlinear evolution of the coalescence instability is found through studies of the electromagnetic particle simulation. The explosive coalescence is a process of magnetic collapse, in which we find the magnetic and electrostatic field energies and temperatures (ion temperature in the coalescing direction, in particular) explode toward the explosion time t_0 as $(t_0-t)^{-8/3}$, $(t_0-t)^{-4}$, and $(t_0-t)^{-8/3}$, respectively. Single-peak, double-peak, and triple-peak structures of magnetic energy, temperature, and electrostatic energy, respectively, are observed on the simulatton as overshoot amplitude oscillations and these features are theoretically explained. Rapid acceleration of particles binormal to the magnetic field and electric field becomes possible.

I. Introduction

The reconnection of field-lines is believed to take place due to finite resistivity $\eta = c^2/4\pi\sigma$ (be it small). The relative magnitude of the time scale for magnetic field-line reconnection may be characterized by the magnetic Reynolds number (or the Lundquist unmber) $R_m = \tau_r/\tau_A$ or a smallness parameter, the inverse of Reynolds number, $\epsilon = R_m^{-1}$. Thus the time scale of reconnection due to the mechanism of the tearing instability is characerized by $\epsilon^{-3/5}$. Sweet and Parker[1] obtained a steady-state solution which has a narrow x-point angle; the time scale τ_{sp} of reconnection is characterized[1] by $\tau_{sp}^{-1} = \eta^{1/2}(n_i/n_e)^{1/2}(v_A/L)^{1/2}1/x_0 \propto \eta^{1/2}$, where $2L$ is the length of the impinged plasma, n_i and n_e are the densities inside and outsidd of the sigular layer.[2] Petschek[3] similarly obtained a steady-state solution which has a large x-point angle; the reconnection time scale τ_p is independent of resistivity, $\tau_p^{-1} \propto \eta^0$. The time scale of reconnection due to the mechanism of the Sweet-Parker process is characterized by $\epsilon^{-1/2}$, while that of Petschek is by ϵ^0. Here we use the words, driven reconnection, in a broad context in which reconnection of magnetic field-lines is incurred so forcibly from external forces that the reconnection process is essentially nonlinear, exhibiting little reminiscent linear instability growth.

In order to rapidly convert magnetic energy into kinetic by a substantial amount, it seems

*Institute for Fusion Studies, University of Texas, Austin, Texas 78712, U.S.A.
**Department of Applied Mathematics and Physics, Toyama University, Toyama, 930 Japan

necessary that the bulk of magnetic energy has to participate in the conversion process: the resistive heating at the x-point alone is too meager. This is because the available magnetic energy at the x-point is smally by itself. On the other hand, the ideal MHD instabilities such as the kink instability and the coalescence instability are the processes that involve the bulk current redistribution in a matter of the Alfvén time scale.

Nonlinear processes of reconnection either driven by external boundary conditions[2,4] or triggered as a secondary process[5] by the primary instability have been investigated. According to Ref.2 for the problem of externally driven reconnection the rate of reconnection experiences more than one phase with a sufficiently strong drive and a compressible plasma: the first Sweet-Parker phase were the reconnected flux $\psi \cong \eta^{1/2}t$ and later (after τ_{sp}) the second phase $\psi \cong \eta^{1/2}t^{\alpha}$, where α is determined by the density compression.

In the present paper and its accmpanying paper[6] we are interested in the latter problem, i.e., the nonlinear driven reconnection triggered as a secondary process by the primary instability. In particular we pick the coalescence instability[7,8] as the primary instability to investigate its nonlinear consequences. We do so because (i) although it is an ideal MHD instability in the linear sense, it would not nonlinearly evolve if there no resistive (non-ideal MHD) effect; (ii) it can involve a large amount of conversion of magnetic to kinetic energes in a short time; (iii) it is essentially a two-dimensional instability, thus more amenable to thorough analysis of the fundamental processes of the intersting to observe that with two-dimensionality restriction we still find an explosive process as we shall see. Generally, it is believed that introductton of an additional dimension (this case, a third dimensin) to the problem allows breaking of symmetry that has been kept before the introduction, leading to more or easier paths to relax the system to the "lowest energy state". Therefore, we should be "guaranteed" to have an explosive process in three dimensions through the nonlinear coalescence instability since it was "already" explosive in two dimensions. In Ref.5 the reconnection was driven by the coalescence instability, the primary instability. The coalescence instability starts from the Fadeev equilibrium[9], which is characterized by the current localization parameter ϵ_c: The equilibrium toroidal current (in the z-direction) is given as $J_z = B_{ox}k(1-\epsilon_c{}^2)\,(\cosh ky + \epsilon_c \cos kx)^{-2}$. The parameter ϵ_c varies from 0 to 1 with small ϵ_c corresponding to a weak localization and ϵ_c close to unity corresponding to a peaked localization; in the limit of $\epsilon_c \to 1$ the current distribution becomes delta function. According to Ref.5 the rate of reconnection was that of Sweet-Parker for small ϵ_c, while the reconnection rate experiences two phases for larger ϵ_c (but smaller than 0.8). This emergence of two phases is similar to the case of the driven reconnection[2]. The intensity of coalescence and the rate of subsequent reconnection are controlled by just one parameter, the current localization (ϵ_c). In this problem there is no ambiguity as to the nature of the driver in contrast to the reconnection driven by external boundary conditions. For the case with $\epsilon_c = 0.7$, the second phase showed the reconnected flux ψ increasing as t^{α} with $1 < \alpha \lesssim 2$. This indicates that the more current localizes, the faster the reconnection becomes.

This leads to a question: Can the reconnected flux ψ increase explosively as $(t_0-t)^{-\alpha}$ ($\alpha > 0$) triggered by the coalescence instability ?

Ⅱ. Explosive Coalescence

In the present section let us show computational results obtained by our electromagnetic particle simulation based on the same parameters as reported in Ref.10 and on a set-up similar to Ref.11. These results show explosive evolution of physical quantities during nonlinear development of the coalescence instability.

Figure 1 displays the time history of various field and particle quantities observed in our simulation in which after the initial transient (up to $t = 4\Omega_i^{-1}$ in the code unit to be explained in the following section) the phase of coalescence of two magnetic islands commences. It is seen in Figs.1(a)-(c) that around $t = 27$ the magnetic and electrostatic field energies shoot up explo-

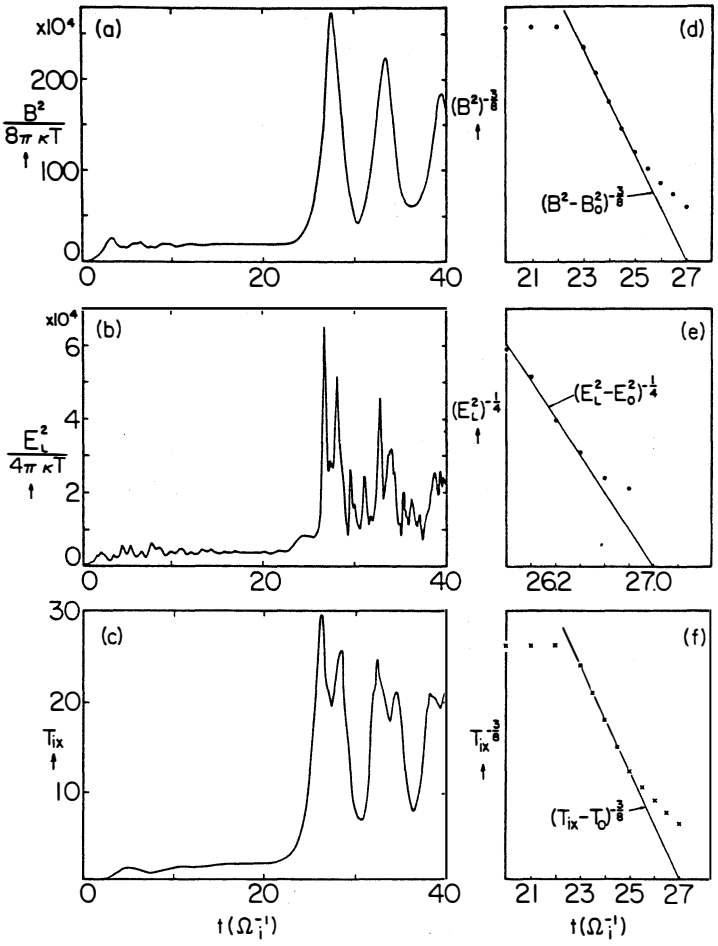

1. Explosive increase of field energies and temperature during the coalescence of two magnetic islands: EM particle simulation results. For the case $\Omega_{et} = 0.2$. Other parameters are given in Sec. Ⅲ. Toward the same explosion time $t = t_0 = 27\,(\Omega_i^{-1})$, tte magnetic energy B^2 (a), electrostatic energy $E_L{}^2$ (b), and the ion temperature in the x-direction T_{ix}(c) diverge as $(t_0-t)^{-8/3}$, $(t_0-t)^{-4}$, and $(t_0-t)^{-8/3}$, as shown in(d), (e), and (f), respectively. [We took $B_0{}^2 \sim 1.6\times10^5$, $E_{L0}{}^2 \sim 7.5\times10^3$, and $T_{ixo} \sim 0.85$ for the pre-explosive phase values; see Figs.1(a)-(c)].

sively as well as the ion temperature in the direction of coalescence (the x-direction). The unit of computational time is omitted hereafter whenever it is unambiguous. It is also seen in Figs.1 (a)-(c) that (i) after the explosive in crease of the field energies and temperature this overshooting results in synchronous amplitude oscillations of all these quantities with the period being approximately the compressional Alfvén period; and (ii) superimposed on these overall amplitude oscillations is a distinct double-peak structure in the electrostatic field energy and the ion temperature. Although we are interested in analyzing the entire episode of the run including the initial phase and the post-explosive phase, we focus particularly on the explosive phase of the coalescence. We replot Figs.1(a)-(c) into Figs.1(d)-(f) to find the way in which these quantities increase toward the catastrophic point. We find from Figs.1(d)-(f) that (i) the magnetic energy explodes as $(t_0-t)^{-8/3}$; (ii) the electrostatic energy explodes as $(t_0-t)^{-4}$; and (iii) the ion temperature in the coalescing direction explodes as $(t_0-t)^{-8/3}$ until saturation due to overshooting sets in, where t_0 is the explosion time measured here to be $t_0 \sim 27\,(\Omega_i^{-1})$ in this run. See Table I.

This discovery of the existence of an explosive process (or instability) and its indices of explosion (the exponent to the time) is important because it tells us that the explosive magnetic process (we may call this the magnetic collapse) can take place in two dimensions and also it prompts our analysis. It is learned that driven reconnection (in the present case it is driven by the coalescence instability) can be explosive under the appropriate conditions. This also underlines a point that the magnetic interaction (the current-current interaction in the manner of Biot-Savart's law) can be inherently attractive and thus explosive (if currents are in the same sense).

TABLE 1 Indices of Explosion [exponents to the $1/(t_0-t)$] During Coalescence

	$\Omega_{et}=0$ $L_x\times L_y$ $=128\times32$ (see Ref. 26) [NB: $L_x\times L_y$ $=256\times32$ many islands]	$\Omega_{et}=0.2\omega_{pe}$ $L_x\times L_y$ $=128\times32$	$\Omega_{et}=1.0$ $L_x\times L_y$ $=128\times32$	$\Omega_{et}=2.0$ $L_x\times L_y$ $=128\times32$ No formation of islands
Magnetic Energy (S) B^2 (T)	8/3 8/3	8/3 8/3	2 2*	N/A
Electrostatic Energy (S) B^2 (T)	4 4	4 4	4	N/A
Ion Temperature in x-direction (S) T_{ix} (T)	8/3 8/3	8/3 8/3	3 2	N/A
Explosive Time (S) t_0	$24.3\Omega_i^{-1}$	$27\Omega_i^{-1}$	$19\Omega_i^{-1}$	N/A
Compressional Alfvén Oscillation Period (S) τ_0	$6.3\Omega_i^{-1}$	$6.0\Omega_i^{-1}$	$8.8\Omega_i^{-1}$	N/A

*incompressibility is assumed. Derivation from observation might be due to plasma rotation in $\Omega_{et}=1$ case.
S is for simulation results and T for theory.

Ⅲ. Particle Simulation

We shall discuss detailed findings of our computer simulation of coalescence of magnetic islands. We present results of a kinetic model of simulation in the present paper. A magnetohydrodynamic simulation along with theorv is presented in the following paper.[6] The results from these two different models are consistent in basic points, but are complementary in many detailed aspects. Here we focus on the particle simulation results.

The kinetic simulation model we abopt here is the electromagnetic particle code[12] with $2\frac{1}{2}$ dimensions. The configuration of the plasma and magnetic field is that of Refs.10 and 11. The plasma density is initially uniform in the x- and y-directions and the z-direction is the ignorable direction. Fields are solvd with periodic boundary conditions in the x-and y-directions. The sheared magnetic fields are generated by the externally imposed sheet currents J_z at $y = 0$ and L_y, where L_y is the lenght of the periodic box in the y-direction. The sheet currents are turned with a ranp function profile in time. The excess of the plasma return current or lack of it for the uniform component (the wavenumber $k = 0$) is compensated by the displacement current term alone, since the term $\nabla \times B$ vanishes for $k = 0$. There narrow slits in x where $J_z = 0$, which fix positions of magnetic islands. The other islands are induced in between the islands that are fixed as mentioned in the above. These islands later coalesce. The process of island generation from this configuration was discussed in Ref.11. The later process of coalescence of generated islands is our main concern in the present article. A uniform external (toroidal) magnetic field B_z is applied with various chosen strenghs. Typical parameters we employ in this code are: the numbers of grid points in the x- and y--directions are $L_x/\Delta = 128$ and $L_y/\Delta = 32$, the number of electrons (and that of ions) 16384, the speed of light $c = 4\omega_{pe}\Delta$, the thermal velocities of electrons in the x-,y-,and z-directions $v_e = 1\omega_{pe}\Delta$, the electron-to-ion mass ratio $m_e/m_i = 1/10$, the electron-to-ion temperature ratio $T_e/T_i = 2.0$, the ("poloidal") sheared magnetic field B_x at $y = 0$ and L_y is such that $eB_x/m_e c = 0.77\omega_{pe}$, and the size of particles $a = 1\Delta$, where Δ is the unit grid length and ω_{pe} is the electron plasma frequency for the uniform plasma at the initial time. The "toroidal" field B_z is varied for various runs with $eB_z/mc\,\omega_{pe}$ ranging from 0 to 0.2,1, and 2.

In these parameters the "poloidal" Larmor radius at the external current sheets for electrons and ions are $\rho_{pe} = 1.2\lambda_{De}$ and $\rho_{pi} = 5.3\lambda_{De}$, the "poloidal" cyclotron frequencies for electrons and ions $\Omega_e = 0.77\omega_{pe}$ and $\Omega_i = 0.077\omega_{pe}$, and the "poloidal" Alfvén velocity $v_{Ap} = 1.22v_e$ and the "poloidal" Alfvén transit time measured in terms of the "poloidal" Alfvén velocity at the sheet with the initial plasma density is $\tau_{Ay} = L_y/v_{Ap} = 26\,\omega_{pe}^{-1}$ and $\tau_{Ax} = L_x/v_{Ap} = 105\,\omega^{-1}_{pe}$. These numbers change accordingly when there is an imposed "toroidal" magnetic field B_z. Because of the nature of the particle code and electromagnetic interactions retained, the temporal and spatial scales of simulation are compressed by using an unrealistically large electron-to-ion mass ratio and small grid. However, it is noted that the main time scales we are interested in are that of the Alfvén time and the electron time scales are sufficiently isolated from this. The chief purpose of this simulation is not to reproduce laboratory plasma behavior but to extract some fundamental underlying processes and try to understand them. In fact, as we shall see, many of the basic characteristics of the simulation findings are reasonably in agreement

with our MHD simulation and explained by theoretical analysis in the companion article.[6]

Figure 2 presents the time history of various field quantities and temperatures in the course of the early fromation and the coalescence process with the toroidal field being such that $eB_z/m_e c \equiv \Omega_{et} = 0.2\omega_{pe}$, while Fig.3 is that with $\Omega_{et} = 1.0\omega_{pe}$. In Fig.2(a) both the magnetic field energy and the ion temperature in the direction of coalescence (x) show that, after the early ($t \leq 3\Omega_i^{-1}$) rise which corresponds to the magnetic island formation by tearing, a long relatively dormant period ($t \cong 3-22$) sets in, followed by a stage ($t \cong 22-27$) of rapid and huge increase in these oscillatory quantities. It is also evident that after the rapid increase ($t \geq 27$) amplitude oscillations ensue in the coalescence due to overshooting. All the other quantities shown in Figs.2(a)-(e) closely follow the pattern of Fig.2(a) with their characteristic events simultaneously occurring. The amplitude oscillations of the tempratues (T_{ix} and T_{iz} as well as T_{ex} and T_{ez}) and the electrostatic field energy have a structure of marked double peaks. The valley of the double-peak structure coincides with the peak of the magnetic field energy ampli-

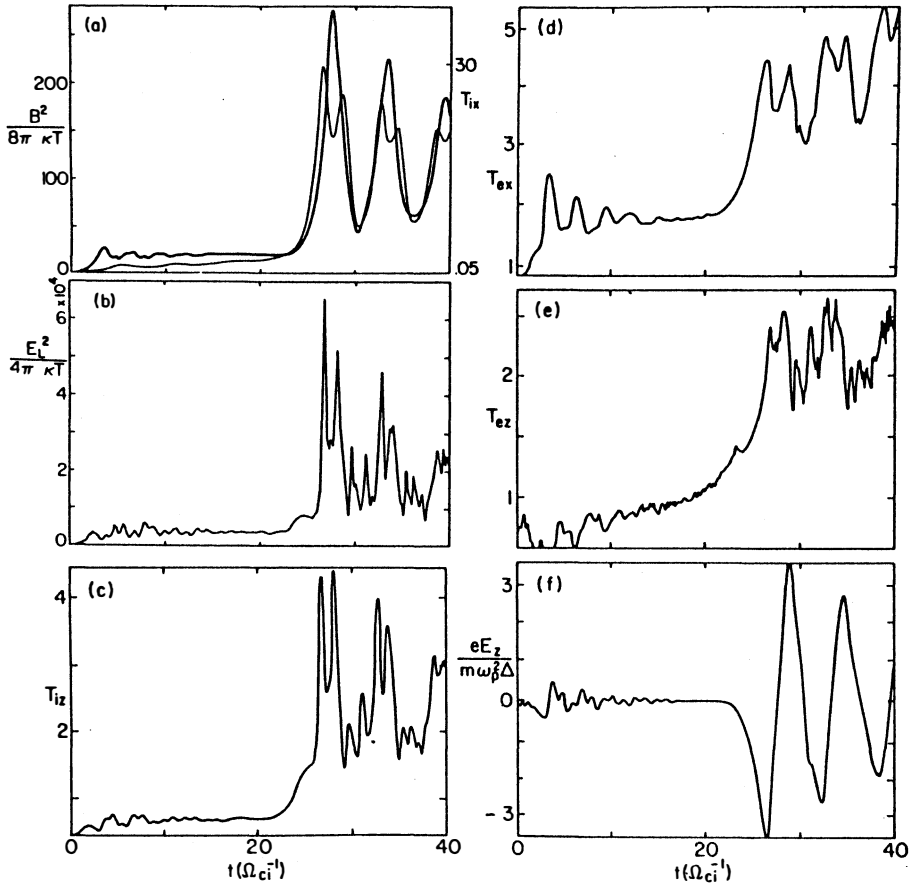

2. Temporal profiles of particle and field quantities for the coalescence process. $\Omega_{et} = 0.2\omega_{pe}$. (a) The thick line represents the magnetic energy, the thin one the ion temperature in the x-directton. (T_{ix} at $t = 0$ was 0.5). (b) Electrostatic field energy in time. (c) Ion temperature in the z-direction. (d) Electron temperature in the x-direction. (e) Electron temperature in the z-direction (f)Inductive electric field (E_z) in time.

tude. As mentioned in Sec.II, it is important to notice that the rapidness of the increase of each quantity differs and that each quantity explosively increases characterized by a certain definite, but different, index of explosion (i.e.,the exponent to the time measured backward from the point of explosion time) until the saturation stage sets in. The early saturation of rise ($t-3$) of each quantity in Figs.2(a)-(e) corresponds to the completion of island formation.[11] The following quiescent period ($3<t\leq 20$) corresponds to the stage where the formed islands slowly attract each other. The rapid explosive rise ($t \geq 20$) marks the commencement of the explosive coalescence. The following stage of amplitude oscillations correspond to the "breathing"[10](or pulsations) of coalesced islands (compressional Alfvén oscillations.) The induced electric field E_z explosively increases when there is rapid flux reconnection during the explosive coalescence and then oscillates as the magnetic flux in the coalesced island is compressed and decompressed.

Figure 3 shows a similar qualitative trend of the coalescence process when the "toroidal field" is stronger ($\Omega_{et} = 1\omega_{pe}$). There are, however, several differences. Although the double-peak structure still appears in most frames of Fig.3, some quantities (the electrostatic field energy and T_{iz}, T_{ez}) do not show clear double peaks anymore. In fact, the electrostatic energy

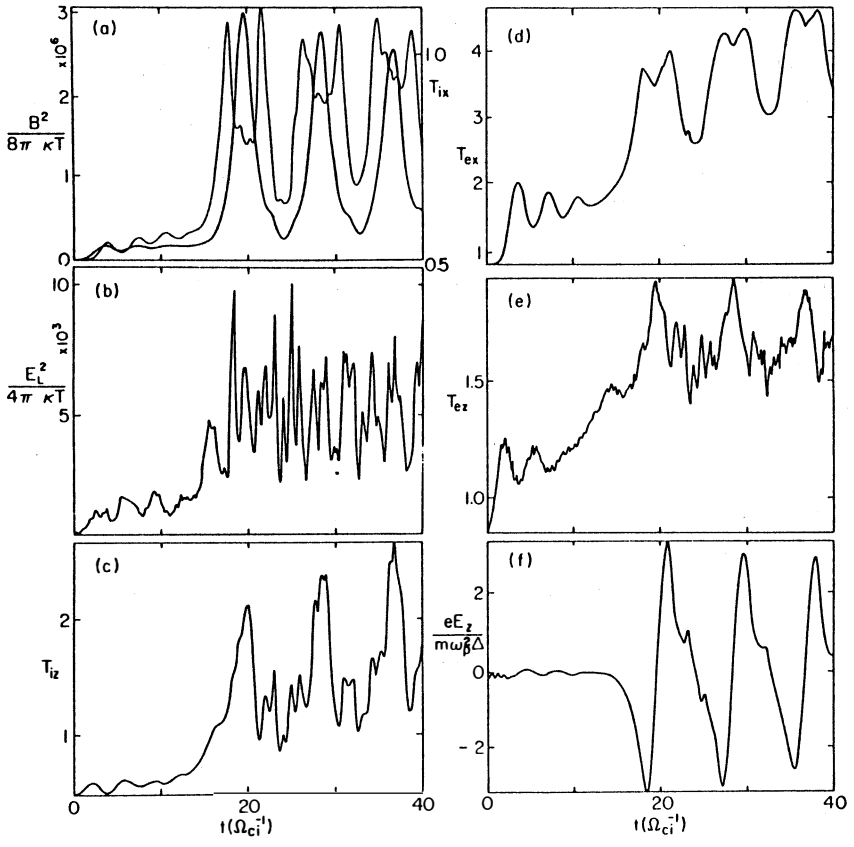

3. Temporal profiles of particle and field quantities for the coalescence with $\Omega_{et} = 1.0$. (a) The thick line for tte magnetic energy, thin line for ion temperature in x. (b) Electrostatic energy. (c) Ion temperature in z. (d) Electron temperature in z. (f) Inductive electric field E_z.

does not show systemtic amplitude oscillations anymore. The period of the amplitude oscillations and the separation of sub-peak in one double-peak structure are longer than in Fig.2.

As the "toroidal field" is further increased to $\Omega_{et} = 2\omega_{pe}$ in this setup, the process of island formation abruptly and qualitatively changes. We called this the threshold phenomenon with the "toroidal" field. The rate of reconnection for island fomation is down by two orders of magnitude and the structure of islands is not coherent but now turbulent. In this case, we did not observe that the system went beyond the stage of early island formation (corresponding to $t \leq 3$ in Fig.2 and 3 cases) within the length of the simulation. (This slow process may correspond to the Sweet-Parker process.[1]) So we do not discuss this case in the present paper. A case with no "toroidal" field case $\Omega_{et} = 0$ was reported earlier,[11] which will also be closely compared with the present cases ($\Omega_{et} = 0.2$ and 1.0).

Let us study the structure of the plasma and fields during the completion of island coalescence. Figure 4 exhibits the spatial structure of the magnetic field lines, the toroidal current density J_z, the plasma electron density, the electron flow, the ion flow, and the electric field at $t = 24\Omega_i^{-1}$, while Fig.5 shows that at $t = 28\Omega_i^{-1}$. In Fig.4(a) the island near $x = 55\Delta$, $y = 16\Delta$ is rapidly approaching the other island at $x = 0$ and $y = 0$ pinned by the sheet current gaps. The former island is accelerated by the intense magnetic fields behind it. The density of electrons is sharply peaked just behind the center of the island [Fig.4(d)]. Electrons flow mainly along the field lines [Fig. 4(d)], while ions which are left behind the electrons try to catch up with the electrons [Fig.4 (e)]. This sets up an electrostatic field pattern with arrows pointing from the inside to the outside of the island [Fig.4(f)]. (Note that in the present code the charge of electrons is taken to be positive for a historical reason.)

On the other hand, Fig.5 presents the case of $\Omega_{et} = 1\omega_{pe}$ just after the coalescence ($t = 18$), corresponding to Fig.3. (The structure before the coalescence is similar to Fig.4.) The electrons flow roughly along the magnetic field lines, but shows some kinks. The ion flow shows a rota-

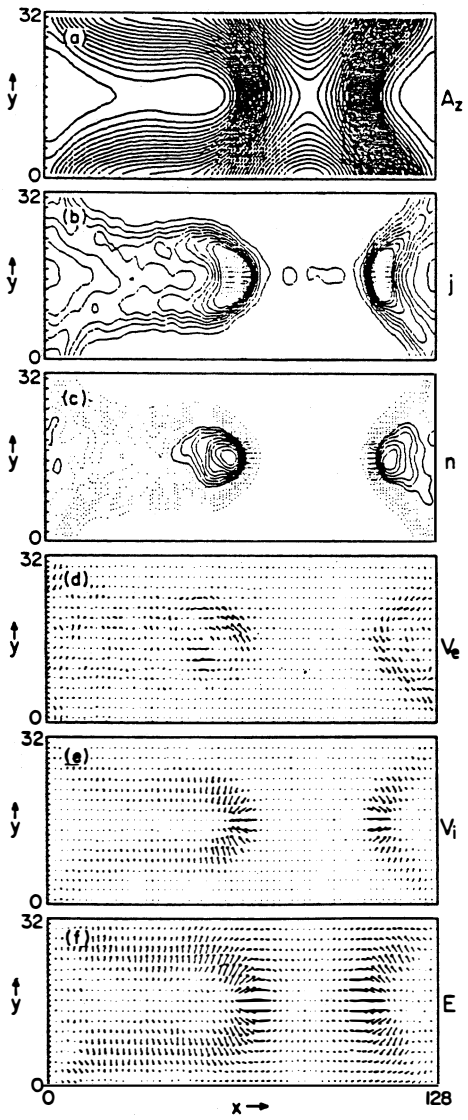

4. Spatial structure of plasma and field before coalescence with $\Omega_{et} = 0.2$ at $t = 24\Omega_i^{-1}$. (a) Magnetic field lines. (b) Current density J_z. (c) Plasma density (d) Electron flow in the x-y-plane (f) Electric fields in the x-y-plane.

tional motion. The main reason for these is that as the "toroidal" magnetic field increases, the incompressibility of the plasma in creases and upon coalescence the island motion adds a strong like $\mathbf{g}\times\boldsymbol{B}_t$, where $\mathbf{g}$ is the acceleration of the islands during the coalescence.

Some of the above findings can be given by a qualitative explanation. Once two currents coalesce, they are bound by the common magnetic flux. The larger coalesced island continues to vibrate. Within the coalesced island the counterstreaming plasma flows cause turbulence which dissipates the flow of energy quickly into heat, thereby reducing the amplitude oscillations of temperatures and fields. As a result, as we shall see, the momentum distribution of plasma electrons and ions exhibit an intense bulk heating and acceleration of the tail. The heating in the poloidal direction (x) is due to adiabatic compression and decompression of the coalesced currents. The eventual bulk heating seems to be a result of turbulent dissipation of counterstreaming instabilities. The heating in the toroidal direction may be due to heating/acceleration by the inductive toroidal electric field which is several times the classical Dreicer field[13] and due to the $v_{ph}\times B$ acceleration. Examination of some of these processes was discussed in Ref.14.

In Fig.6 we show heating and acceleration of particles during the coalescence. The particle acceleration in the high energy tail of ions and electrons is qualitatively discussed here. The tail formation is probably due to a combination of localized electrostatic field acceleration across the "poloidal" magnetic field[15] and magnetic acceleration ($v_p\times B$ acceleration). A plasma and field behavior similar to that shown in Fig.4 persists up to $t\sim t_1\sim 27\,\Omega_i^{-1}$. Electrons are magnetized and are carried away with the accelerating magnetic flux, while bulk ions are accelerated by the $J\times B$ force. On the other hand, the high energy ions are due to the charge separation created near the compressed flux. The difference of motions between ions and electrons around $t=t_1$ causes a strong localized shock-like electrostatic field, E_L, whose phase propagates with a phase velocity of the structure $v_{ph}=v_x$. Here the mechanism of $v_p\times B$ acceleration is that an electrostatic wave propagating with phase velocity

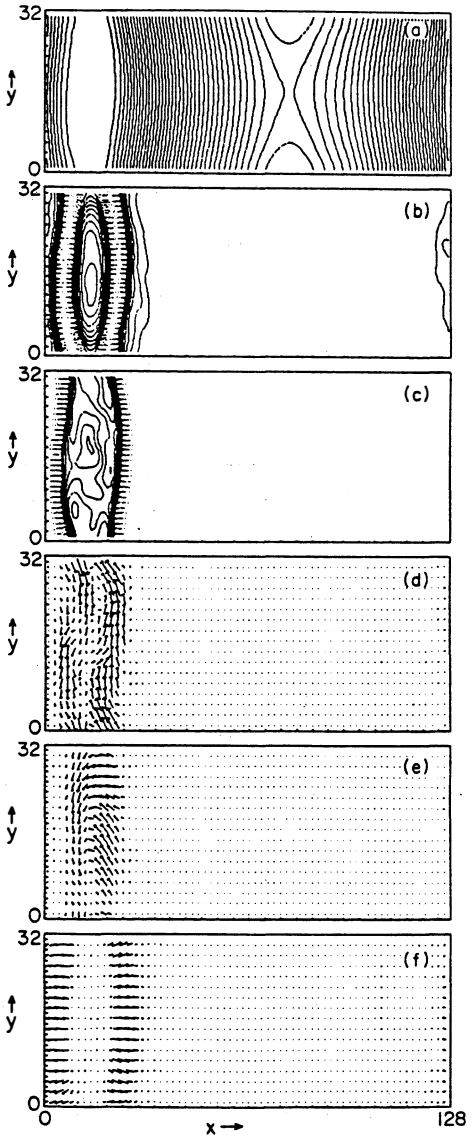

5. Spatial structure of plasma and fields during coalescence with $\Omega_{et}=1$ at $t=18\Omega_i^{-1}$. (a)~(f) as indicated for Fig.4.

v_p can add energy to a particle that is propagating obliquely to the wave propagation direction by combining the electric acceleration and $v_p \times B$ acceleration when the particle is trapped in the wave. This $v_p \times B$ acceleration[15] causes the formation of high energy particles in the "toroidal" direction. By this acceleration process, ions and electrons are accelerated to relativistic energies in oppsite directions along the toroidal magnetic field.

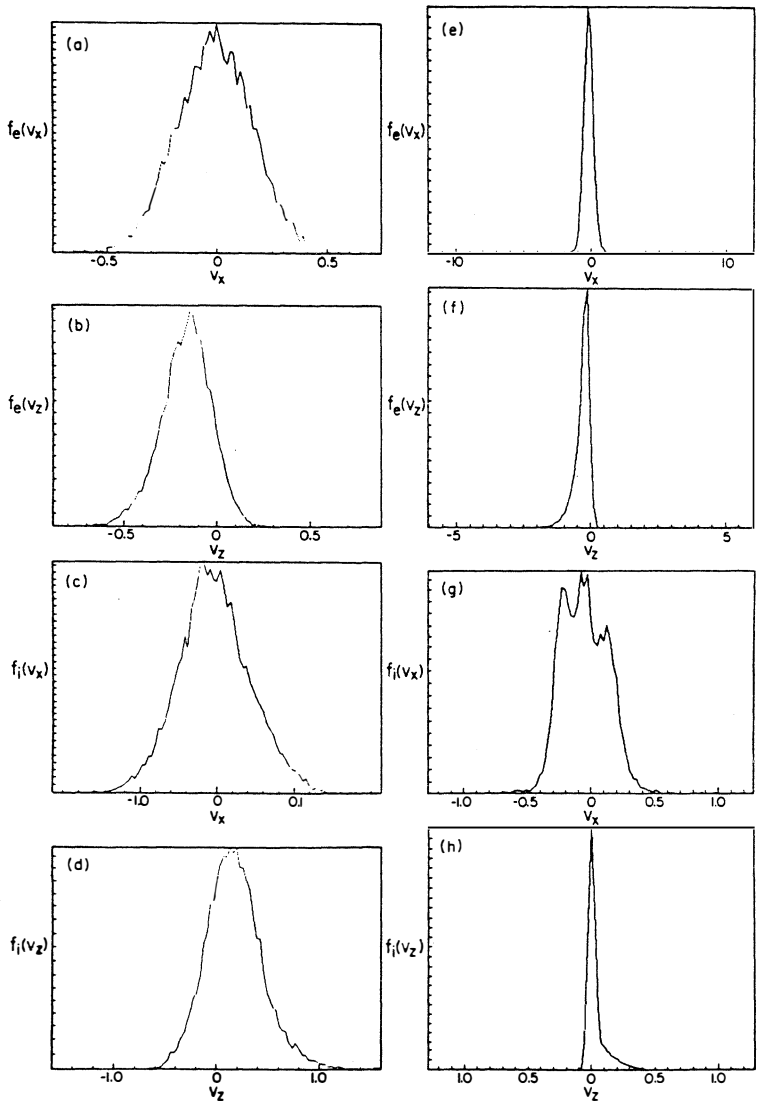

6. Disribution functions of electrons and ions "before" [(a)-(d)] and "after" [(e)-(h)] coalescence. (a)-(d) at $t = 24\Omega_i^{-1}$ and (e)-(h) at $t = 28\Omega_i^{-1}$. (a) and (e) the electron velocity distribution in the x-direction. (b) and (f) the electron velocity distribution in the z-direction. (c) and (g) the ion velocity distribution in the x-direction. (d) and (h) the ion velocity distribution in the z-direction. Note that unit for velocities on the left frames is $\omega_p\Delta$, while those on the right is c. The electron momenta are measured in $m\omega_p\Delta$ (or $M\omega_p\Delta$ for ions) on the left, while those on the right in mc (or Mc for ions).

IV. Discussion

We have found that in the magnetic collapse the electrostatic field can be explosively generated and can grow more rapidly than the magnetic field. [The explosiveness of the electrostatic field $E_x \sim (t_0-t)^{-2}$, and magnetic field $B_y \sim (t_0-t)^{-4/3}$]. The kinetic simulation finds that, in the explosive phase, ions and electrons are simultaneously accelerated in the z-direction, opposite each other. When a particle moves across the magnetic field driven by the electrostatic field E_x, the particle can be accelerated in a direction (z-direction) perpendicular both to the electric field (x-direction) and the "poloidal" magnetic field (y-direction). This acceleration mechanism was considereed by Sagdeev and Shapiro,[15] by Sugihara et al.[16] and Dawson et al.[17]

By slightly stretching the present theory of explosive coalescence in two dimensions we may be able to discuss the process of tokamak major disruption.[18] The explosive process we find in the coalescence instability is characterized by singular functions of time with a pole (or a branch point) at the explosion time $(t_0-t)^{-m}$. The tokamak major disruption has been modeled as nonlinear evolution of unstable tearing and/or resistive kink modes (mainly the $m = 2, n = 1$ mode and $m = 3, n = 2$) and their destabilization of other beat modes such as the $m = 5, n = 3$mode and its coupling to higher m and n's. It is interesting to extract from their numerical simulation[19] that the toroidal voltage approximately scales as $(t_0-t)^{-2}$ toward the disruption time t_0 to our best fit (Fig.5 of Ref.19). The toroidal voltage is related to E_z in the present paper, which has power exponents of 7/3 and 5/3 close to 2. The exponent γ itself explodes as $(t_0-t)^{-2}$ to our best fit, suggesting an approximate functional form of exp $[(t_0-t)^{-1}]$ for the kinetic energy. From this study of Fig.3 of Ref.19 the singularity of the temporal explosion of the major disruption is characterized by an essential singularity. In their model the electrostatic potential ϕ and the magnetic flux ψ obey equations with quadratic nonlinearity. With single helicity calculations it seems not possible for us to construct temporal functions with an essential singularity. However, with multiple helicities interacting with each other it may be possible to argue that a strongly developed turbulence which is established by a cascade of many higher order best modes gives rise to an essential singularity in the temporal behavior: secondary processes yielding $(\phi,\psi) \propto (t_0-t)^{-2}$, tertiary processes (beats of beats) $\propto (t_0-t)^{-3}$, quartic processes $\propto (t_0-t)^{-4}$,.... With a certain combinatorial arrangement which depends on individual dynamics of turbulence, one sums up the entire energy as $\sum_{n=0}^{\infty} C_n (t_0-t)^{-n}$, where C_n's are cofficients; the analytic property of such a function may be generically related to that of exp $[(t_0-t)^{-1}]$.

We would like to thank Drs. J.N.Leboeuf, J.M. Dawson, and A.G. Litvak for fruitful discussions. This work is supported by the U.S. Department of Energy and the National Science Foundation.

References

1. P.A. Sweet, in *Electromagnetic Phenomena in Cosmic Physics* (Cambridge Univ. Press, London, 1958), p.123; E.N. Parker, J. Geophys. Res. **62**, 509(1957).
2. F. Brunel, T. Tajima, and J.M. Dawson, Phys. Rev. Lett. **49**, 323(1982).

3. H.E. Petschek, Proc. AAS-NASA Syprosium on Physics of Solar Flares (NASA SP-50, 1964) p.425.
4. T. Sato and T. Hayashi, Phys. Fluids **22**, 1189(1979).
5. A. Bhattacharjee, F. Brunel, and T. Tajima, Phys. Fluids **26**, 3332(1983).
6. T. Tajima and J.I. Sakai, accompanying paper.
7. J.M. Finn and P.K. Kaw, Phys. Fluids **20**, 72(1977).
8. P.L. Pritchett and C.C. Wu, Phys. Fluids **22**, 2140(1979).
9. V.M. Fadeev, I.F. Kvartskawa, and N.N. Komarov, Nucl. Fusion **5**, 202(1965).
10. T. Tajima, F. Brunel, and J.-I. Sakai, Ap. J. **245**, L45(1982).
11. J.N. Leboeuf, T. Tajima, and J.M. Dawson, Phys. Fluids **25**, 784(1982).
12. A.T. Lin, J.M. Dawson, and H. Okuda, Phys. Fluids **17**, 1995(1974).
13. H. Dreicer, Phys. Rev. **115**, 238(1959).
14. J.I. Sakai and T. Tajima, in *Proc. Joint Varenna-Abastumani International School and Workshop on Plasma Astrophysics* (EAS, Sukhumi, 1986) **SP256**, p.113.
15. R.Z. Sagdeev and V.D. Shapiro, JETP Lett. **17**, 279(1973).
16. R. Sugihara and Y. Midzuno, J. Phys. Soc. Jpn. **47**, 1290(1979).
17. J.M. Dawson, et al., Phys. Rev. Lett. **50**, 1455(1983).
18. L.A. Artsimovich, Nucl. Fusion **12**, 215(1972).
19. P.H. Diamond, R.D. Hazeltine, Z.A. An, B.A. Carreras, and H.R. Hicks, Phys. Fluids **27**, 1449 (1984).

(Received October, 31 1988)